0013-4651/2011/158(9)/H915/4/$28.00 © The Electrochemical Society

Inverted Octagonal Surface Defects in *a*-Plane AlGaN/GaN Multiple Quantum Wells

Huei-min Huang, Chiao-yun Chang, Tien-chang Lu,[z] and Chi-chin Yang

Department of Photonics and Institute of Electro-Optical Engineering, National Chiao Tung University, Hsinchu 30050, Taiwan

The structural properties of *a*-plane AlGaN/GaN multiple quantum wells grown on the *r*-plane sapphire substrate have been characterized. The pentagonal and inverted octagonal surface pits, consisting of several non-polar and semi-polar crystalline facets, are clearly observed and distinguished. The Al incorporation efficiency of the non-polar and semi-polar facets of these special inverted octagonal surface pits has been verified in the order of $(11\bar{2}2) < (10\bar{1}2) < (1\bar{1}00) \approx (11\bar{2}0) < (20\bar{2}1)$ by cathodoluminescence measurements at room temperature. The evolution of these inverted octagonal surface pits could be due to the results of interaction between different stacking faults.
© 2011 The Electrochemical Society. [DOI: 10.1149/1.3610990] All rights reserved.

Manuscript submitted March 8, 2011; revised manuscript received June 22, 2011. Published July 15, 2011.

Growth of GaN-based materials along non-polar orientations such as *a*-axis [1120] (Ref. 1) and *m*-axis [1100] (Ref. 2) has been demonstrated as an effective approach to solve the influence of quantum confined stark effect.[3] Compared with conventional *c*-plane nitrides, growth of non-polar nitrides suffers from higher defect density. Recently, the most important issue for crystal quality improvement of non-polar nitrides is to understand the defect generation. The surface imperfection, surface pits[4–6] and existence of large amounts of structural defects such as basal stacking faults (BSFs) and partial dislocations[7–9] have held back the advantageous property of non-polar nitrides. It is well-known that density of BSFs is evaluated as high as 10^5 cm^{-1} and dislocation density is about 10^{10} cm^{-2} for non-polar nitrides grown either on *r*-plane sapphire or γ-$LiAlO_2$ substrates. Typically, these BSFs are either terminated by partial dislocations or connected to neighboring BSFs by the prismatic stacking faults (PSFs).[10,11] Additionally, anisotropic crystal island and surface pits are commonly observed due to the anisotropic epitaxial growth rate in different orientations. The relative growth rates of different semi-polar crystalline facets of wurtzite structure are important factors in evolution of surface pits. For example, the commonly observed pentagonal pits in *a*-plane GaN could gradually evolve into triangular shapes.[12] In this study, we analyzed the structural and surface defects of non-polar *a*-plane AlGaN/GaN MQWs. The special inverted octagonal surface defects have been distinctly observed by scanning electron microscopy (SEM) images. The emission spectra of each crystalline orientation by performing CL measurements have been taken to study the Al incorporation efficiency of the non-polar and semi-polar facets. Thus, the evolution of these inverted octagonal surface pits was discussed.

Experimental

Ten periods *a*-plane AlGaN/GaN MQWs consisted of 10 nm-thick AlGaN barriers and 3.5 nm-thick GaN wells. The MQWs structure was grown in atmosphere of N_2 at 1100°C on a GaN template by low-pressure metal-organic chemical vapor deposition. The *in situ* SiN_x interlayer was inserted between the *r* plane sapphire substrate and GaN template to improve the GaN template crystalline quality. During the growth, trimethylgallium and trimethylaluminum were used as group III source materials and ammonia as the group V source material. The high-resolution x-ray diffraction (HRXRD) was utilized to analyze the AlGaN composition and to determine the well and barrier thickness. Further, the strain state of AlGaN/GaN MQWs was investigated by asymmetric XRD reciprocal space mappings (RSMs). The cross section TEM measurements revealed distribution and microstructure of defects. CL measurements were carried out at room temperature (300 K) by using the Gatan MonoCL system equipped in the JEOL-7000F FE-SEM. The electron beam with acceleration voltage of 10 kV had a beam size of ~10 nm and the penetration depth of ~0.7 μm for characterization of QWs on surface pits. The electron probe current was kept at 10 nA.

[z] E-mail: timtclu@mail.nctu.edu.tw

Results and Discussion

Figure 1a shows the HRXRD $\omega-2\theta$ scan of *a*-plane AlGaN/GaN MQWs taken on GaN $(11\bar{2}0)$ reflection. Not only does the scan profile reveal strong diffraction from the GaN layer, but also satellite peaks are clearly observed to the third order, which can be used to determine the MQWs structural parameters including the Al composition of $Al_xGa_{1-x}N$ barrier and the thicknesses of quantum well. The Al composition in the barrier was determined to be 0.18, while the thicknesses of well and barrier were about 3.5 and 10 nm, respectively. The appearance of the higher order satellite peaks implied a good periodic quantum well structure. In order to study strains in *a*-plane AlGaN/GaN MQWs, the asymmetric RSM on $(02\bar{2}0)$ has been measured. The main two peaks shown in Fig. 1b are clearly observed. The lower peak is determined as GaN diffraction and the upper one is AlGaN diffraction. The diffraction peak of AlGaN is aligned with that of GaN template along the same Q_x for $(02\bar{2}0)$ mappings, indicating that AlGaN and GaN have the same lattice constant and the AlGaN/GaN MQWs structure is almost fully strained without relaxation.

The defect structures of AlGaN/GaN MQWs were observed including line, planar and volume defects by different zone-axis cross section TEM images. These TEM images were taken along the $[1\bar{1}00]$ and [0001] zone axis orientation, respectively. Besides, individual selected area diffraction (SAD) patterns were taken and shown in Figs. 2a and 2c. For the $[1\bar{1}00]$ zone axis orientation (Figs. 2a and 2b), BSFs are clearly observed as thin lines aligning in parallel with [0001] *c*-axis direction. The BSFs propagate from below the GaN epilayer grown on a foreign substrate towards AlGaN barriers and GaN quantum wells. The density of BSFs was estimated about 1×10^5 cm^{-1}. In addition, the asymmetric V-shaped faceted pit is observed, and it consists of an inclined facet and a vertical $(000\bar{1})$ sidewall, as shown in Fig. 2b. The inclined facet makes an angle of about 30° with the [0001] *c*-axis direction, and it could be either $(11\bar{2}2)$ or $(20\bar{2}1)$ facets. It is interesting to note that the MQWs structure is still grown on the facet of V-shaped pit. Figures 2c and 2d show the cross section TEM images along the [0001] zone axis direction. For this zone axis, the threading dislocations, PSFs and some rectangular voids are clearly observed. The rectangular void is a kind of three dimensional defects as indicated in Fig. 2c. The formation mechanism of these voids associate with folded stacking fault domains. Figure 2d shows the visible PSFs inclined at about 60° to the surface direction and formed along the $(\bar{2}110)$ and $(1\bar{2}10)$ as thin lines [indicated by arrows]. Some of PSFs intersect with each other and propagate to the sample surface. According the analyzed results, the density of dislocation is estimated about 5×10^9 cm^{-2}, which is lower than the

Downloaded on 2014-04-24 to IP 140.113.38.11 address. Redistribution subject to ECS terms of use (see ecsdl.org/site/terms_use) unless CC License in place (see abstract).

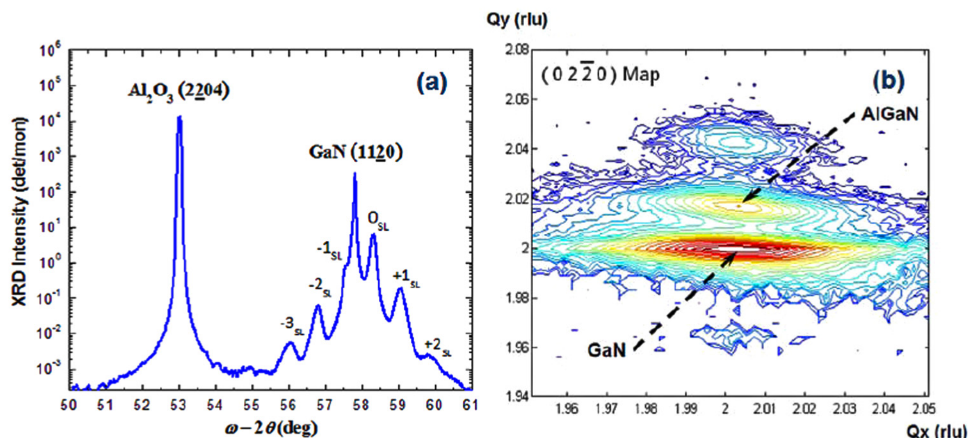

Figure 1. (Color online) (a) HRXRD omega/2theta scan and (b) asymmetric reciprocal-space mapping of $(02\bar{2}0)$ reflection for *a*-plane AlGaN/GaN MQWs structure grown on *r*-plane sapphire substrate.

previous reports,[13,14] and can be corresponding to the slight strain relaxation in AlGaN/GaN MQWs demonstrated in the RSM measurement.

The incomplete island coalescence phenomenon found in Fig. 2b has also been observed by the SEM measurement. The top view SEM images in Fig. 3 show the typical pentagonal surface pit aligned along c-axis direction. The intersection angle between the two crystal planes is about 135°, formed by the $(10\bar{1}2)$ facet. The other faceted types for pentagonal surface pit have been identified as $(11\bar{2}2)$ and $(20\bar{2}1)$, respectively. Figure 3b shows the perspective view SEM image. Several crystalline planes such as $(10\bar{1}1)$, $(10\bar{1}3)$ and (0001) have been clearly observed and identified, as shown in the magnification image of Fig. 3c. Furthermore, as shown in Fig. 4a, the special inverted octagonal surface pits consisted of several non-polar and semi-polar crystalline facets have been observed. Each different non-polar and semi-polar crystalline facets of this pit are marked according to the results provided by Sun et al.[12,15–17] Compared with typical triangular and pentagonal surface pits commonly decorating the *a*-plane GaN-based material, this kind of surface pit has never been reported up to now.[12,18] Hence, we further studied and clarified the characteristics of AlGaN/GaN MQWs structure in the inverted octagonal surface pits by CL measurements, which have been widely used to study defect-related emissions.[19,20]

Figure 4b shows the CL spectra from each distinct facet of the inverted octagonal surface pit. The dashed line in Fig. 4b is the *a*-plane GaN emission energy at room temperature (3.42 eV). Thus, the peak energy at 3.492 eV shown in Fig 4b is attributed to the emission from $(11\bar{2}0)$ *a*-plane AlGaN/GaN MQWs. In addition, the $(1\bar{1}00)$ *m* facet emission spectrum is similar to the $(11\bar{2}0)$ plane and the relative weak emission peak at 3.826 eV corresponds to (Al, Ga)N barriers. The dominant peak in the $(10\bar{1}2)$ facet emission reveals a red shift of about 21 meV compared to the emission peak from $(11\bar{2}0)$ plane. It could be due to the decrease of Al

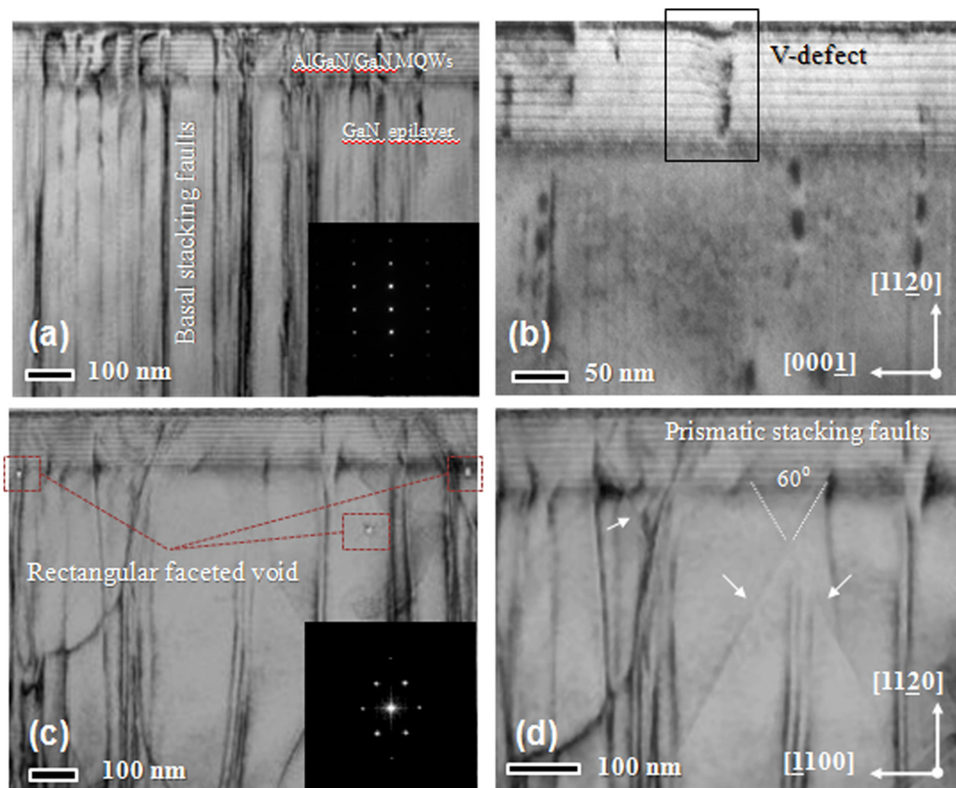

Figure 2. (Color online) Cross section of bright-field transmission electron microscopy images for *a*-plane AlGaN/GaN MQWs structure taken along the $[1\bar{1}00]$ (a–b) and [0001] (c–d) zone axes, respectively.

Downloaded on 2014-04-24 to IP 140.113.38.11 address. Redistribution subject to ECS terms of use (see ecsdl.org/site/terms_use) unless CC License in place (see abstract).

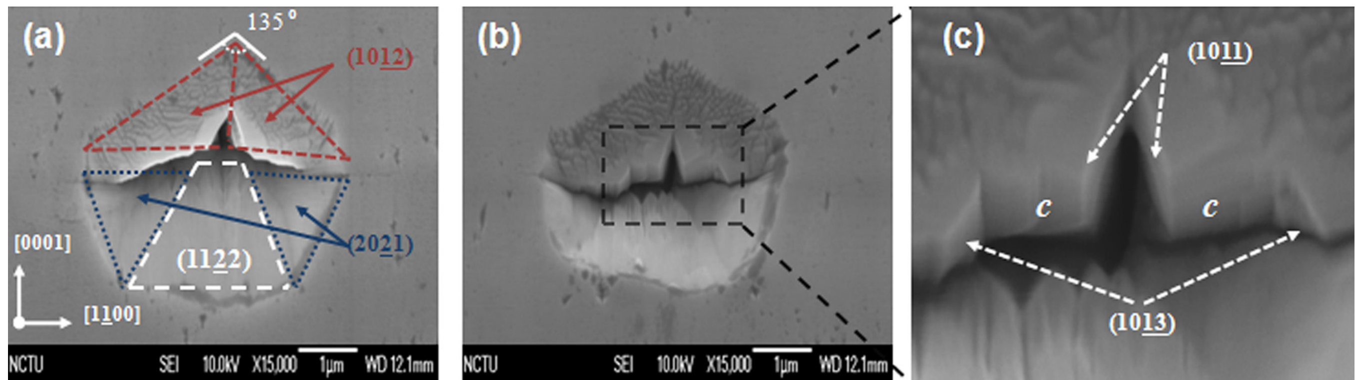

Figure 3. (Color online) (a) Top view and (b) perspective view (45° inclined from *a*-axis to in-plane *c*-axis) scanning electron microscopy images for the pentagon-like surface pit of *a*-plane AlGaN/GaN MQWs structure. (c) Magnified image of (b).

incorporation efficiency, leading to slight reduction of the quantum confinement effect. This can also be proved by the red-shift of (Al, Ga)N barriers emission peak from original 3.826 to 3.702 eV. In the emission spectrum from the $(11\bar{2}2)$ facet, the MQW peak at 3.425 eV and (Al, Ga)N barrier peak at 3.595 eV have been determined. A large amount of red shift in (Al,Ga)N barriers emission indicates relatively low Al incorporation efficiency on the $(11\bar{2}2)$ facet. However, the emission spectrum from the $(20\bar{2}1)$ facet shows a dominant peak at 3.554 eV. The relatively large blue shift of the emission energy could be due to the increase of Al content and the decrease of quantum well thickness, simultaneously.[21–23] The Al incorporation efficiency of each crystal facet can be determined in the order of $(11\bar{2}2) < (10\bar{1}\bar{2}) < (1\bar{1}00) \approx (11\bar{2}0) < (20\bar{2}1)$. It should be noted that although the Al incorporation efficiency on non-polar and semi-polar AlGaN/GaN MQWs is a key factor to clarify the CL spectrum peak shift, the variation of the quantum well thickness on the different crystalline facets is also an important issue to affect the CL spectrum peak shift.

Moreover, the CL spectrum was taken while the excitation electron beam was focused in the central diamond-shaped void, and the electron beam with acceleration voltage of 10 kV corresponded to a beam size of ∼10 nm and penetration depth of ∼0.7 μm. It is shown in Fig. 4b that the dominant emission energy at 3.35 eV is lower than the *a*-plane GaN bulk emission energy (3.42 eV), indicating that this optical transition does not occur in AlGaN/GaN MQWs. Instead, it could be attributed to the emission from the intersection between PSFs and BSFs in the *a*-plane GaN template.[24,25] Due to the PSFs have very large fault energy, it dissociates into two low-energy BSFs with accommodation of the difference between fault vectors at each of two BSF/PSF intersections by a stair-rod dislocation.[8] Since the stair-rod dislocation is expected at the intersection of these two stacking faults, the generation of inverted octagonal surface pits in *a*-plane GaN could be associated with the interaction of these two stacking faults according to the measurement result.

Conclusions

In summary, we have investigated the structural defects of non-polar *a*-plane AlGaN/GaN MQWs structure. The pentagonal and inverted octagonal surface pits, consisting of several non-polar and semi-polar crystalline facets, are clearly observed. The Al incorporation efficiency is very different on the non-polar and semi-polar facets due to different emission energies in CL measurements. The evolution of inverted octagonal surface pits could be associated with the interaction between PSFs and BSFs in the GaN template. These

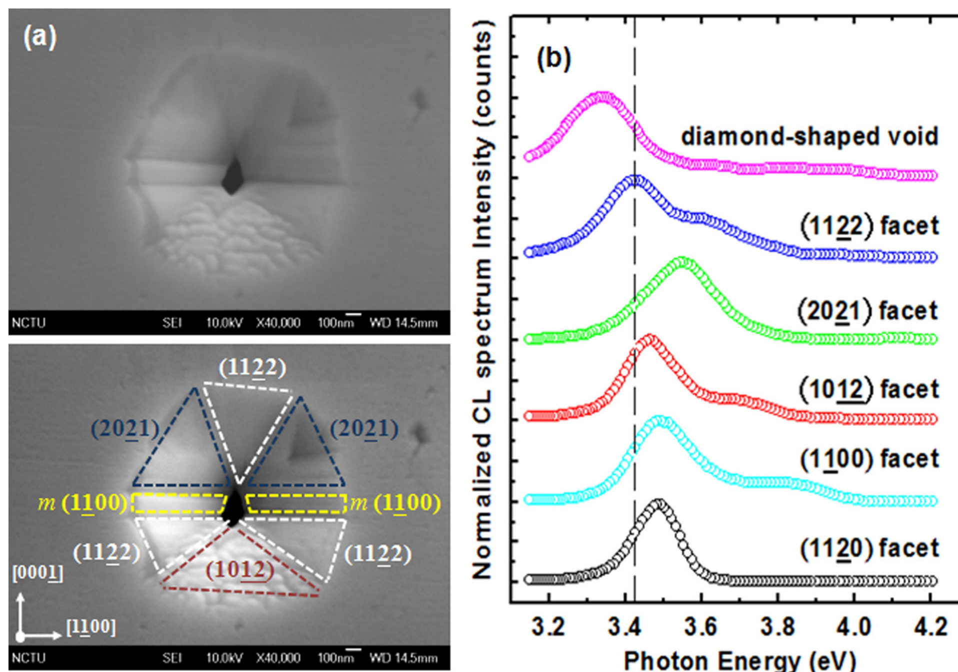

Figure 4. (Color online) (a) Top view SEM images and (b) the CL spectra from each distinct surface of the inverted octagonal surface pit in *a*-plane AlGaN/GaN MQWs structure.

Downloaded on 2014-04-24 to IP 140.113.38.11 address. Redistribution subject to ECS terms of use (see ecsdl.org/site/terms_use) unless CC License in place (see abstract).

results shall be beneficial to clarify the emissions from non-polar and semi-polar facets within surface pits.

Acknowledgments

These works were supported by the MOE ATU program and in part by the National Science Council of Republic of China (ROC) in Taiwan under contract No. NSC-99-2120-M-009-007 and NSC-96-2221-E-009-035-MY3. Prof. S. C. Wang and Prof. H. C. Kuo are sincerely acknowledged for helpful discussion and collaboration.

References

1. M. D. Craven, S. H. Lim, F. Wu, J. S. Speck, and S. P. DenBaars, *Appl. Phys. Lett.* **81**, 1201 (2002).
2. P. Waltereit, O. Brandt, M. Ramsteiner, A. Trampert, H. T. Grahn, J. Menniger, M. Reiche, R. Uecker, P. Reiche, and K. H. Ploog, *Phys. status solidi A*, **180**, 133 (2000).
3. P. Waltereit, O. Brandt, A. Trampert, H. T. Grahn, J. Menniger, M. Ramsteiner, M. Reiche and K. H. Ploog, *Nature (London)*, **406**, 865 (2000).
4. M. D. Craven, F. Wu, A. Chakraborty, B. Imer, U. K. Mishra, S. P. DenBaars, and J. S. Speck, *Appl. Phys. Lett.*, **84**, 1281 (2004).
5. T. S. Ko, T. C. Wang, R. C. Gao, H. G. Chen, G. S. Huang, T. C. Lu, H. C. Kuo, and S. C. Wang, *J. Cryst. Growth*, **300**, 308 (2007).
6. J. L. Hollander, M. J. Kappers, C. McAleese, and C. J. Humphreys, *Appl. Phys. Lett.*, **92**, 101104 (2008).
7. B. A. Haskell, F. Wu, M. D. Craven, s. Matsuda, P. T. Fini, T. Fujii, K. Fujito, S. P. DenBaars, J. S. Speck, and S. Nakamura, *Appl. Phys. Lett.*, **83**, 644 (2003).
8. D. N. Zakharov, Z. Liliental-Weber, B. Wagner, Z. J. Reitmeier, E. A. Preble and R. F. Davis, *Phys. Rev. B*, **71**, 235334 (2005).
9. J. Mei, S. Srinivasan, R. Liu, F. A. Ponce, Y. Narukawa, and T. Mukai, *Appl. Phys. Lett.*, **88**, 141912 (2006).
10. T. Paskova, R. Kroeger, S. Figge, D. Hommel, V. Darakchieva, B. Monemar, E. Preble, A. Hanser, N. M. Williams, and M. Tutor, *Appl. Phys. Lett.*, **89**, 051914 (2006).
11. P. Vennéguès, Z. Bougrioua, and T. Guehne, *J. Appl. Phys.*, **46**, 4089 (2007).
12. Q. Sun, C. D. Yerino, T. S. Ko, Y. S. Cho, I. H. Lee, J. Han, and M. E. Coltrin, *J. Appl. Phys.*, **104**, 093523 (2008).
13. M. D. Craven, P. Waltereit, J. S. Speck, and S. P. DenBaars, *Appl. Phys. Lett.*, **84**, 496 (2004).
14. T. J. Badcock, P. Dawson, M. J. Kappers, C. McAleese, J. L. Hollander, C. F. Johnston, D. V. Sridhara Rao, A. M. Sanchez, and C. J. Humphreys, *Appl. Phys. Lett.*, **93**, 101901 (2008).
15. Q. Sun, Y. S. Cho, I. H. Lee, J. Han, B. H. Kong, and H. K. Cho, *Appl. Phys. Lett.*, **93**, 131912 (2008).
16. Q. Sun, B. H. Kong, C. D. Yerino, T. S. Ko, B. Leung, H. K. Cho, and J. Han, *J. Appl. Phys.*, **106**, 123519 (2009).
17. Q. Sun and J. Han, Proc. SPIE, **7617**, 761717 (2010).
18. F. Wu, M. D. Craven, S. H. Lim and J. S. Speck, *J. Appl. Phys.*, **94**, 942 (2003).
19. R. Liu, A. Bell, F. A. Ponce, C. Q. Chen, J. W. Yang, and M. A. Khan, *Appl. Phys. Lett.*, **86**, 021908 (2005).
20. K. J. Fujan, M. Feneberg, B. Neuschl, T. Meisch, I. Tischer, K. Thonke, S. Schwaiger, I. Izadi, F. Scholz, L. Lechner, et al., *Appl. Phys. Lett.*, **97**, 101904 (2010).
21. N. Grandjean, B. Damilano, S. Dalmasso, M. Leroux, M. Laugt, and J. Massies, *J. Appl. Phys.*, **86**, 3714 (1999).
22. M. Esmaeili, H. Haratizadeh, B. Monemar, P. P. Paskov, P. O. Holtz, P. Bergman, M. Iwaya, S. Kamiyama, H. Amano, and I. Akasaki, *Nanotechnology*, **18**, 025401 (2007).
23. A. Hangleiter, F. Hitzel, C. Netzel, D. Fuhrmann, U. Rossow, G. Ade, and P. Hinze, *Phys. Rev. Lett.*, **95**, 127402 (2005).
24. P. P. Paskov, R. Schifano, B. Monemar, T. Paskova, S. Figge, and D. Hommel, *J. Appl. Phys.*, **98**, 093519 (2005).
25. P. P. Paskov, R. Schifano, T. Malinauskas, T. Paskova, J. P. Bergman, B. Monemar, S. Figge, D. Hommel, B. A. Haskell, P. T. Fini, et al., *Phys. Status Solidi C*, **3**, 1499 (2006).

Downloaded on 2014-04-24 to IP 140.113.38.11 address. Redistribution subject to ECS terms of use (see ecsdl.org/site/terms_use) unless CC License in place (see abstract).